British Journal of Applied Science & Technology
4(1): 1-17, 2014

SCIENCEDOMAIN *international*
www.sciencedomain.org

Histological Imaging of Gastric Tumors by Scanning Acoustic Microscope

Katsutoshi Miura[1*] and Seiji Yamamoto[2]

[1]Departments of Health Science, Pathology and Anatomy, Hamamatsu University School of Medicine, 1-20-1 Handa-yama, Higashi-ku, Hamamatsu 431-3192, Japan.
[2]Medical Photonics Research Center, Hamamatsu University School of Medicine, 1-20-1 Handa-yama, Higashi-ku, Hamamatsu 431-3192, Japan.

Authors' contributions

This work was carried out in collaboration between all authors. Author KM designed the study, performed the statistical analysis, wrote the protocol, and wrote the first draft of the manuscript and managed literature searches. Author SY prepared the microscopic equipment and managed the analyses of the study. All authors read and approved the final manuscript.

Research Article

Received 2nd June 2013
Accepted 21st August 2013
Published 1st October 2013

ABSTRACT

Background: Human body tissues have their own speed-of-sound (SOS) by which sound travels through them. Harder materials exhibit greater SOS; thus, SOS through each tissue can provide information regarding its elasticity. For tumor discrimination in clinical medicine, palpation provides important information. However, manual palpation is subjective, whereas SOS data are objective and can be directly used to compare lesions.
Methods: A scanning acoustic microscope (SAM) uses ultrasound to image an object from SOS through tissues. We investigated the utility of SAM in imaging gastrointestinal lesions.
Results: We visualized the digestive tract as a layered structure and discriminated tumors to a degree comparable with that observed by light microscopy. Areas with greater SOS corresponded to those with higher collagen or muscle fiber concentrations. Cell-poor areas or regions with degeneration demonstrated less SOS than surrounding tissues. Gastric tumors displayed appropriate SOS similar to their original tissues and showed significant differences in SOS between scirrhous carcinomas and well-differentiated medullary carcinomas, scirrhous carcinomas and malignant lymphomas, and leiomyomas and leiomyosarcomas.

**Corresponding author: E-mail: kmiura@hama-med.ac.jp;*

Conclusions: SAM offered the following benefits over LM: (1) images are acquired in a few minutes without special staining; (2) repeated observations of the same section are possible; (3) high-resolution digital imaging from SOS is comparable to LM; (4) SAM analysis could be helpful in understanding endoscopic ultrasonography imaging; and (5) digitized SOS data could be statistically compared among different stomach lesions.

Keywords: Scanning acoustic microscope; tissue elasticity; cancer imaging; gastric tumor; fibrosis.

1. INTRODUCTION

Humans possess two major sensory organs, the eyes and ears, which facilitate vision and hearing, respectively. Material discrimination by light microscopy (LM) has been useful in elucidating various cell systems, although sound has been rarely used in medical science. Some mammals, such as bats and dolphins, use high-frequency (>20 KHz) ultrasound (US) for chasing game.

Human body tissues have their own speed-of-sound (SOS) by which sound travels through them. Harder materials exhibit greater SOS; thus, SOS through each tissue can provide information on its elasticity [1]. For tumor discrimination in clinical medicine, palpation provides important information: most sarcomas are softer than carcinomas, and scirrhous carcinomas are harder than medullary carcinomas. However, manual palpation is subjective and depends on experience, whereas SOS data is objective and can be directly used to compare lesions.

Endoscopic ultrasonography (EUS) has recently become a popular option for observing deep submucosal or deeper lesions, such as cancer invasion, submucosal tumors, and lymph node metastasis in the gastrointestinal (GI) tract [2,3]. However, EUS is macroscopic and cannot be used to predict histology.

A scanning acoustic microscope (SAM) is a device that uses US frequency (>80 MHz) to microscopically image an object [4]. We recently reported that SAM could be used to generate useful information about lung [5] and lymph node [6] lesions.

Can SAM visualize GI normal structures? How are lesions detected by SAM? Does SOS really correspond to tissue elasticity? Is SAM superior to LM?

Here, we show representative SAM gastric images and discuss its utility for clinical diagnosis.

2. MATERIALS AND METHODS

2.1 Materials

All materials from anonymous donors were prepared from the Hamamatsu University Hospital archives. The research protocol using stored samples without link to patient identity was approved by the research ethics committee of Hamamatsu University School of Medicine. Formalin-fixed, paraffin-embedded (FFPE) blocks were flat-sectioned in 10-μm thick sections. Because deparaffinized sections repeled water due to surface hydrophobicity and dried out easily, it was necessary to soak sections enough in distilled water to reduce

hydrophobicity. So deparaffinized unstain sections were soaked in distilled water for at least 3 h before observation. Continuous sections were stained with hematoxylin & eosin (H & E) for comparison of SAM images with corresponding light microscopy (LM) images.

2.2 Tissue Samples

We examined and selected normal and neoplastic stomach lesions, including adenocarcinomas (well or poorly differentiated), carcinoid tumors, GI stromal tumors (GISTs), leiomyomas, malignant lymphomas, leiomyosarcomas, and schwannomas.

2.3 SAM Observation

The SAM was supplied by Honda Electronics (Toyohashi, Japan) and was equipped with a 120-MHz transducer, which has a resolution of approximately 13 μm (Fig. 1). SAM functions by directing focused sound from a transducer to a small area of the target object on a glass slide. The sound emitted by an acoustic transducer hits or penetrates the tissue and is reflected on the surface of the tissue or glass. It is then returned to the receiver, which is coincident with the transducer. The SOS through the tissue is automatically calculated by comparing the time-of-flight of the pulse from the surfaces of both tissue and glass.

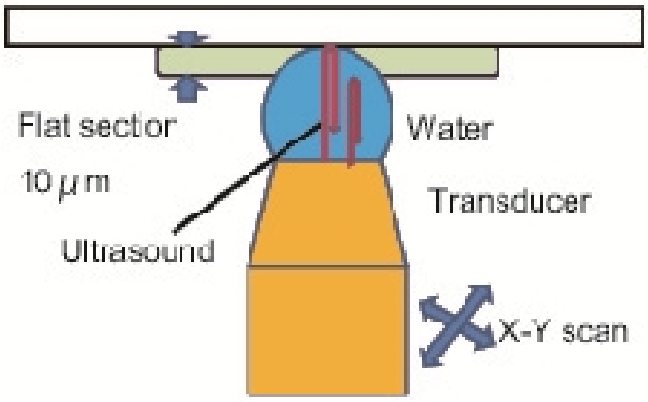

Fig. 1. Principles of scanning acoustic microscopy (SAM)

Ultrasonic waves from the transducer reflect off both the glass slide and the section and return to the transducer. These waves pass through 10-μm sample sections with different ultrasonic properties. The transducer automatically scans the section to calculate the speed-of-sound through each area. The section is placed upside down on the transducer, and distilled water is applied between the transducer and the section as a coupling fluid. The control speed-of-sound (SOS) through water is 1500 m/s.

To perform SAM imaging, the slide sections were placed upside-down on the stage above the transducer, and distilled water was applied between the transducer and the section as a coupling fluid; this was done because air interferes with sound transmission. After mechanical X–Y scanning, SOS from each point on the section was calculated and plotted on the screen to create two-dimensional, color-coded images (Fig. 2A). The vertical bar on the left and the horizontal bar at the bottom of each figure indicate the distance (mm) on the slide. The vertical colored column on the right side of the figure indicates the average SOS of each square area on the section. The region of interest (ROI: 1.2, 2.4, or 4.8 mm^2) for acoustic microscopy was determined from the LM images. SOS values at 300 × 300 points were calculated and plotted on the screen to create the images, and sound data from 64 cross points on the lattice screen were used for statistical analysis.

Other data such as thickness of the section and sound attenuation were also available from each point and were shown on the screen (data not shown).

2.4 Statistical Analysis

SOS data from each tissue element are presented as mean ± standard deviation (SD; m/s). Student's *t*-tests were used to determine statistically significant differences among the specimens. The level of statistical significance was set at $P < 0.01$.

3. RESULTS

3.1 Normal Gastric Structure

From the inner to outer surfaces, normal gastric layers consist of mucosa, lamina muscularis mucosae (MM), submucosa (SM), muscularis externa (ME), subserosa, and serosa. The SAM system can effectively discriminate among these gastric layer structures (Fig. 2A). In the mucosa, foveolar and glandular structures were well visualized by SAM (Fig. 2B).

Cell-rich areas displayed greater SOS than cell-deficient areas. MM displayed linear band structure with greater SOS and showed a clear boundary with SM. Smooth muscle layers, including MM and ME, exhibited greater SOS than the mucosal layer (Table 1, Fig. 3).

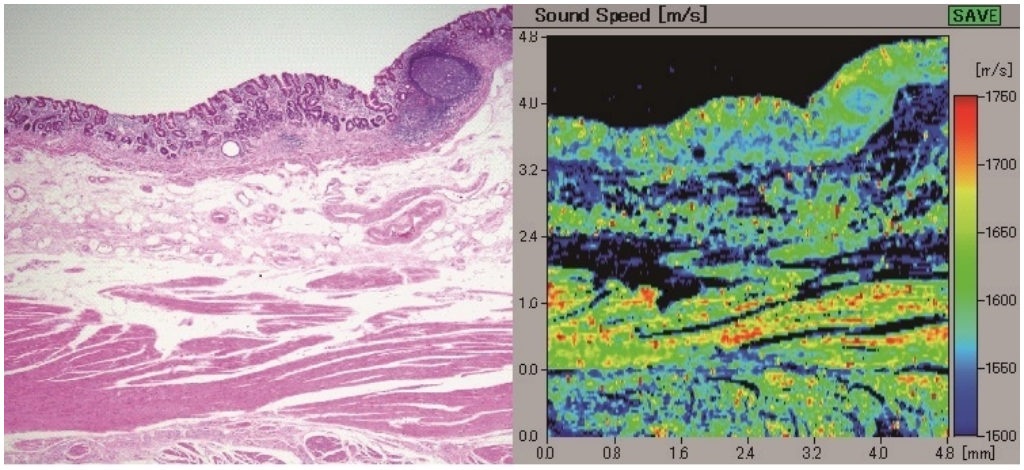

Fig. 2A. Scanning acoustic microscopy imaging of normal stomach tissue

From top to bottom, the gastric wall consists of the mucosa, the lamina muscularis mucosae (MM), the submucosa (SM), the muscularis externa (ME), and the serosa. The acoustic image (right) clearly discriminates these layer structures comparable with its corresponding H&E-stained light microscopy image (left). The speed-of-sound values of the thick ME is highest among these layers.

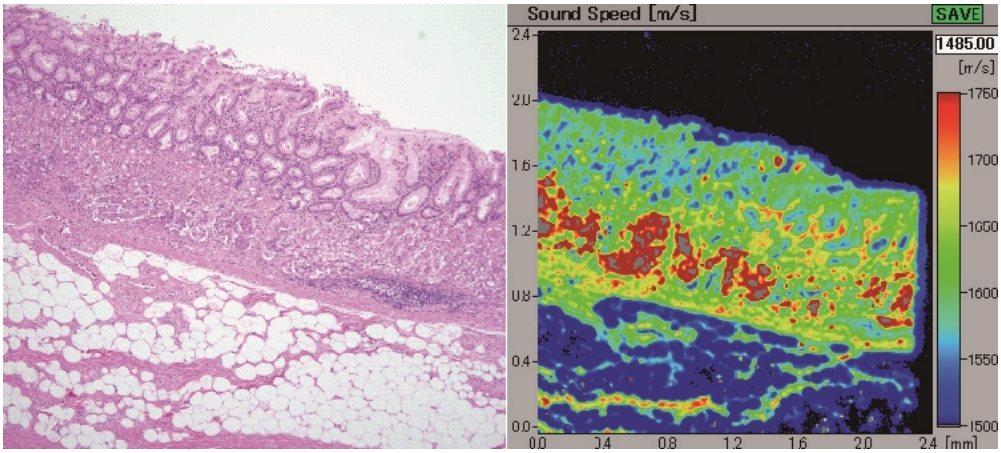

Fig. 2B. The acoustic image (right) of normal gastric mucosa and submucosa and its corresponding light microscopic image with H&E staining (left)

Foveolar and glandular structures are clearly visualized by scanning acoustic microscopy. The cell-rich area shows higher speed-of-sound (SOS) than the cell-deficient area. The muscularis mucosae exhibit a linear, thin-banded structure with higher SOS. In the submucosa, blood and lymph vessels show narrow tubular structures with greater SOS.

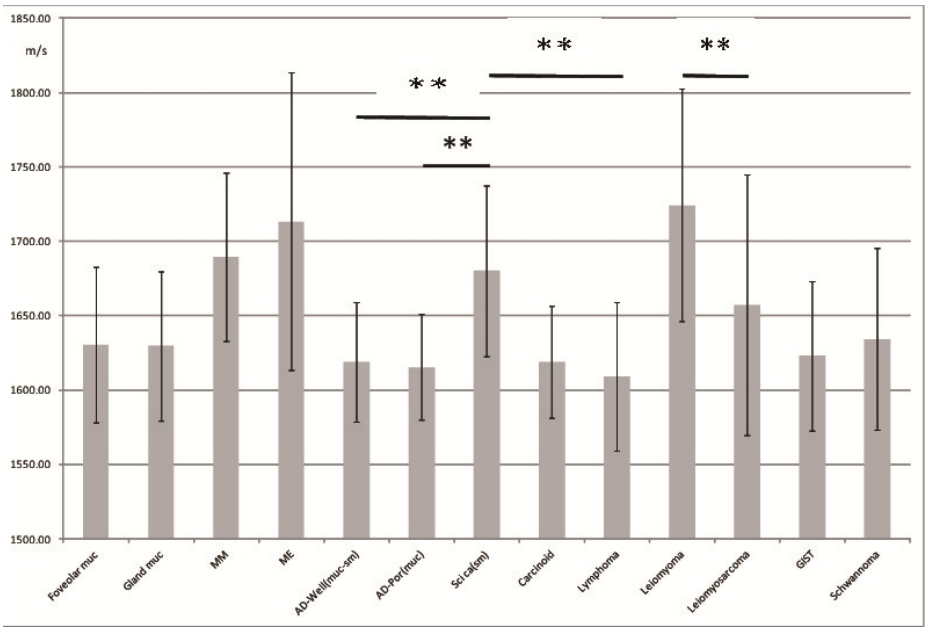

Fig. 3. The mean and SD (m/s) of speed-of-sound through gastric location are shown

*Foveolar muc, foveolar mucosa; Gland muc, glandular mucosa; MM, muscularis mucosae; ME, muscularis externa; AD-Well(muc-sm), well-differentiated adenocarcinoma (mucosa, submucosa); AD-Por(muc), poorly differentiated adenocarcinoma (mucosa); Sci ca (sm), scirrhous carcinoma (submucosa); GIST, gastrointestinal stromal tumor, ** P < 0.01.*

Table 1. The mean speed-of-sound through gastric location (m/s), SD and reference range

Location	n	AVE	SD	RR lower	RR upper
Foveolar muc	105	1630.51	52.14	1528.32	1732.7
Gland muc	53	1629.58	49.97	1531.64	1727.52
MM	57	1689.47	56.43	1578.87	1800.07
ME	90	1713.34	99.97	1517.39	1909.28
AD-Well(muc-sm)	155	1618.89	40.32	1540.09	1697.68
AD-Por(muc)	91	1615.36	35.67	1545.45	1685.27
Sci ca(sm)	210	1680.05	57.52	1567.32	1792.78
Carcinoid	59	1619.08	37.66	1545.27	1692.89
Lymphoma	196	1608.93	49.87	1511.19	1706.67
Leiomyoma	162	1724.30	78.38	1570.68	1877.92
Leiomyosarcoma	113	1657.07	87.72	1485.14	1829
GIST	171	1622.96	50.18	1524.61	1721.31
Schwannoma	68	1634.27	61.09	1514.54	1754

Foveolar muc, foveolar mucosa; Gland muc, glandular mucosa; MM, muscularis mucosae; ME, muscularis externa; AD-Well(muc-sm), well-differentiated adenocarcinoma (mucosa, submucosa); AD-Por(muc), poorly differentiated adenocarcinoma (mucosa); Sci ca (sm), scirrhous carcinoma (submucosal invasion); GIST, gastrointestinal stromal tumor; RR lower, lower reference range; RR upper, upper reference range.

3.2 Carcinomas of the Stomach

Well and poorly differentiated adenocarcinomas arising from the mucosa formed tubular structures and signet-ring cells, respectively (Figs. 4A, 4B). The SOS of adenocarcinomas was low, which was identical to that of normal mucosa. No significant difference was observed between well and poorly differentiated carcinomas in the mucosa (Table 1, Fig. 3).

At sumucosal invasive sites, well-differentiated adenocarcinoma with medullary growth exhibited SOS which were the same as that of the original mucosa (Fig. 4C), while poorly differentiated scirrhous carcinoma exhibited greater SOS than normal mucosa (Figs. 4D and 4E). The SOS values of scirrhous carcinomas were significantly higher than well-differentiated carcinoma with medullary growth (Fig. 3, Table 1).

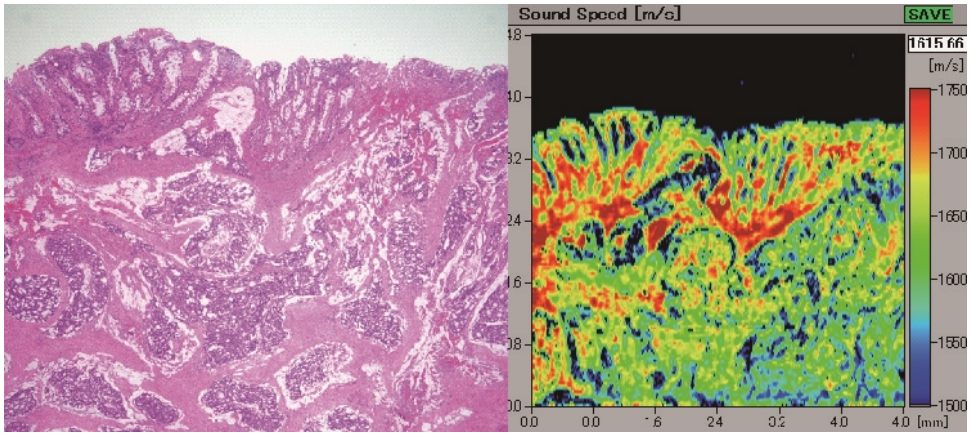

Fig. 4A. A well-differentiated adenocarcinoma with mucosal spread
Irregular tubular structures with fused glands are shown among normal foveolar tubules from the right upper to the left lower areas in the figure. Smooth muscles in the muscularis mucosae separate the clusters of cancer cells with conspicuous speed-of-sound values.

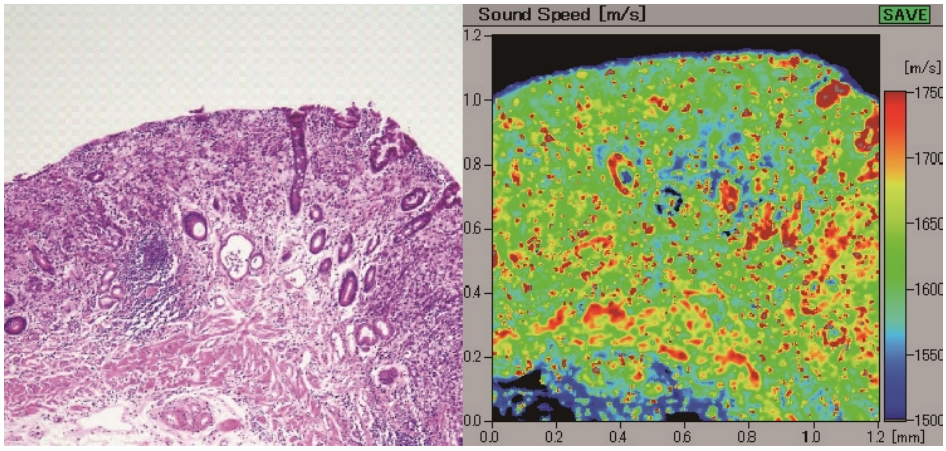

Fig. 4B. A poorly differentiated adenocarcinoma spreading through the mucosa
The normal foveolar and glandular structures have disappeared and are replaced by signet ring cells that are represented as scattered dots with increased speed-of-sound values (right).

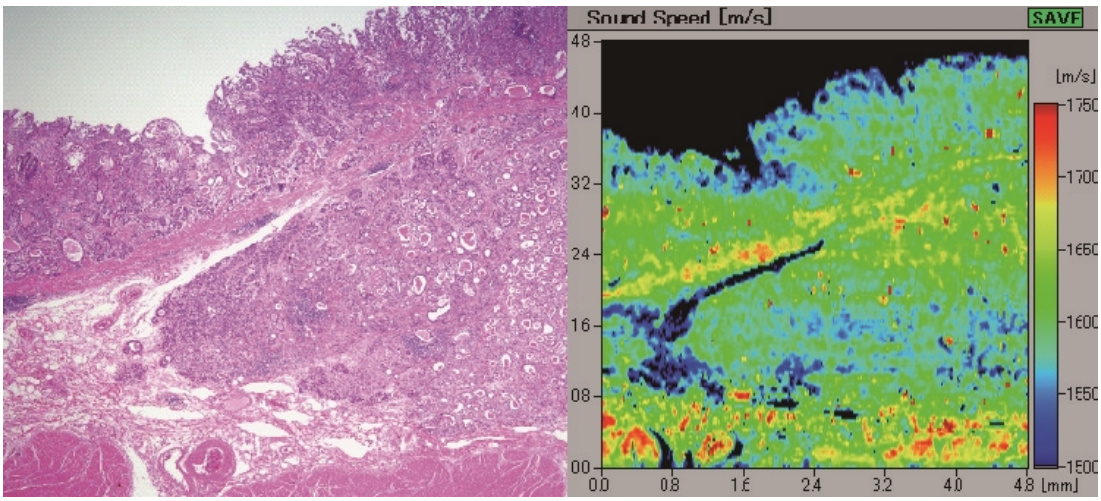

Fig. 4C. A well to moderately differentiated adenocarcinoma invading from the mucosa to the submucosa with medullary growth

The normal tubular architecture is replaced by cancer cells. The smooth muscle layer of muscularis mucosae is split (arrow) by invading cancer.

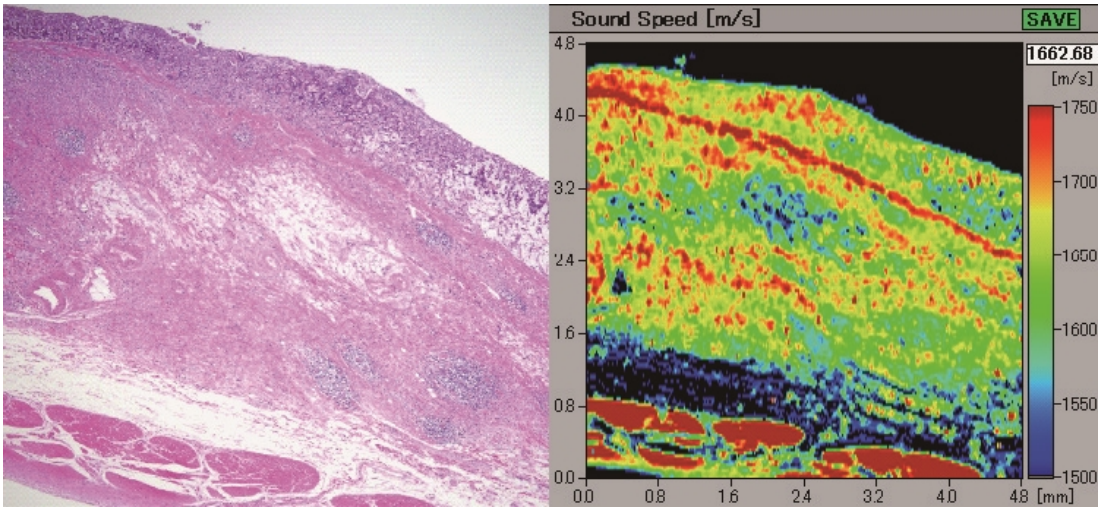

Fig. 4D. A poorly differentiated adenocarcinoma with scirrhous submucosal invasion

Many signet ring cells spread in the mucosa and infiltrate beyond the muscularis mucosae into the submucosa. In the submucosa, desmoplastic reactions with collagen fiber proliferation are seen, and spicular structures exhibit greater speed-of-sound.

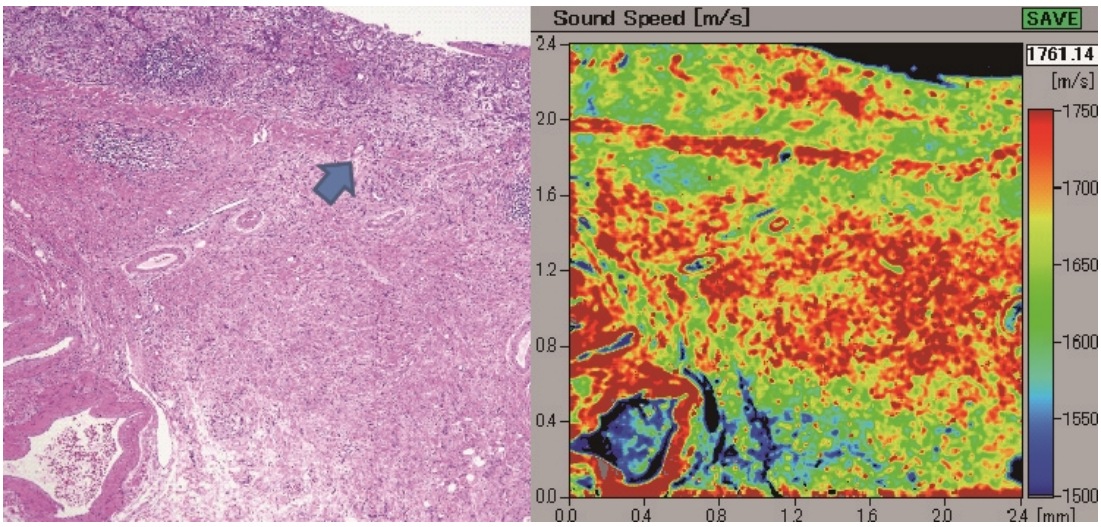

Fig. 4E. A poorly differentiated adenocarcinoma with scirrhous spread

Many signet ring cells infiltrate from the mucosa to the submucosa with desmoplastic reactions, which demonstrate speed-of-sound similar to that observed in muscularis mucosae or perivascular smooth muscle. An arrow indicates split smooth muscles of the muscularis mucosae.

3.3 Carcinoid Tumors of the Stomach

Carcinoid tumors consisting of trabecular structure with scarce stroma showed less SOS than the surrounding mucosa (Fig. 5).

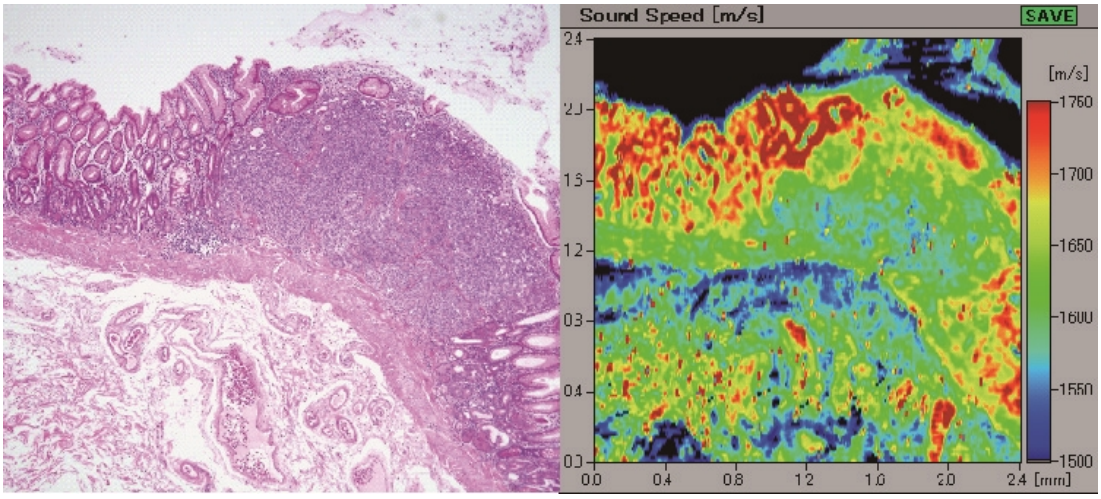

Fig. 5. A small gastric carcinoid tumor in the mucosa

The carcinoid portion consisting of trabecular structure with scant fibrous components exhibits lower speed-of-sound than the surrounding mucosa (right).

3.4 Malignant Lymphomas

Malignant lymphoma displayed the least SOS of all assessed tumors (Fig. 6A and 6B, Table 1). The SOS values of the lymphomas were significantly lower than those measured in scirrhous carcinoma samples (Fig. 3).

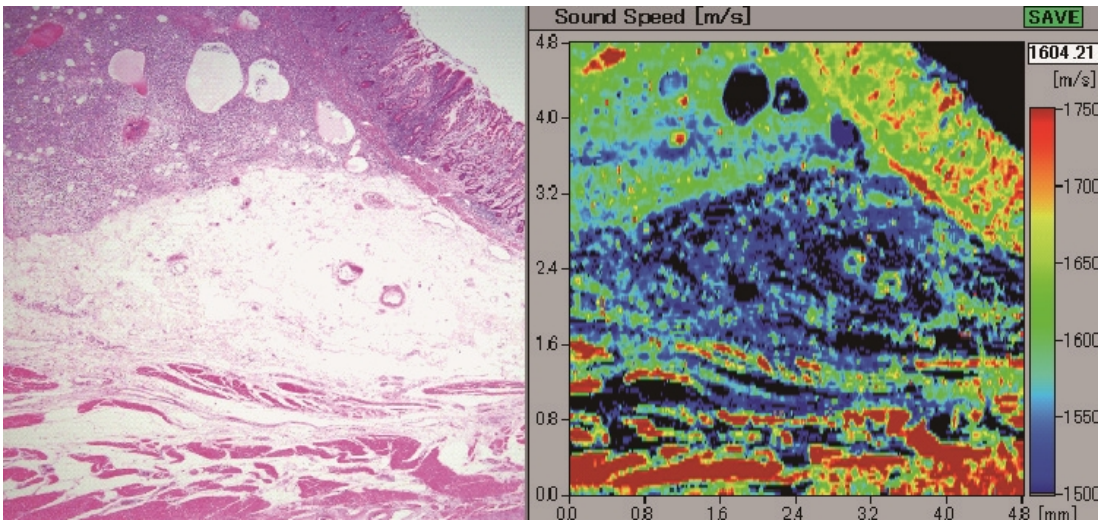

Fig. 6A. A gastric malignant lymphoma infiltrating from the mucosa to the submucosa
The lymphoma shows reduced speed-of-sound and spreads among mucosal tubules (right).

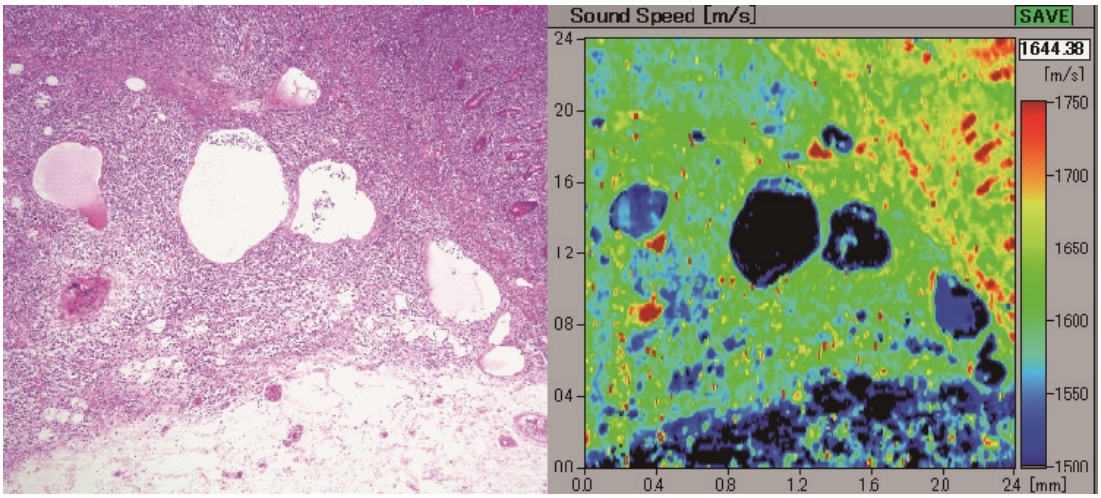

Fig. 6B. Higher magnification of the gastric lymphoma shown in Fig. 6A
The lymphomatous area exhibits the least speed-of-sound (SOS) among the mucosal components. The dilated lymph vessels and the congested veins in the lymphoma show lower and higher SOS, respectively.

3.5 Leiomyomas and Leiomyosarcomas

Leiomyomas appeared as sharp nodular structures and demonstrated SOS values as high as those of smooth muscles of MM, ME, and blood vessels (Figs. 7A and 7B, Table 1). Thick muscle bundles exhibited the greatest SOS values (Fig. 7C).

Leiomyosarcoma with great SOS area showed geographic myxoid degeneration with less SOS area (Fig. 8A), and their transitions were abrupt and irregular. Multinodular leiomyosarcoma with high cellularity displayed less SOS compared with septal fibrous bands (Fig. 8B). The SOS values of leiomyosarcomas were significantly lower than those of leiomyomas (Fig. 3).

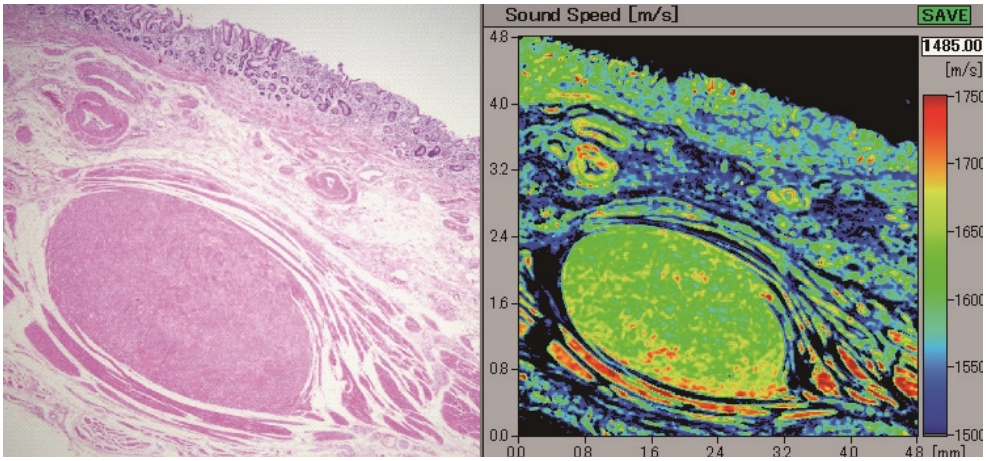

Fig. 7A. A gastric leiomyoma in the ME

An elliptical leiomyoma with clear margins shows speed-of-sound (SOS) similar to that of the smooth muscles of muscularis mucosae, ME, and blood vessel walls. The surrounding ME displays higher SOS due to compression artifact.

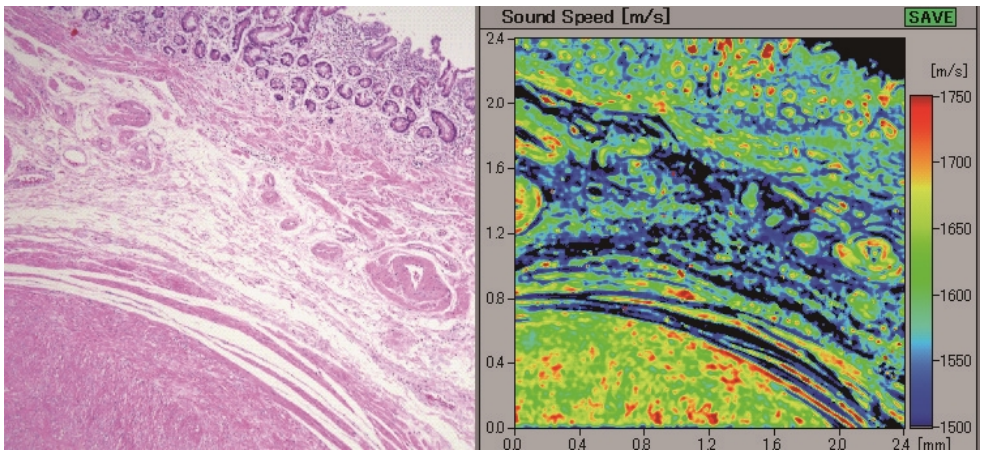

Fig. 7B. Higher magnification of the leiomyoma shown in Fig. 7A

The higher speed-of-sound areas in the right scanning acoustic microscopy image correspond to dense fascicles of smooth muscle and interstitial blood vessels.

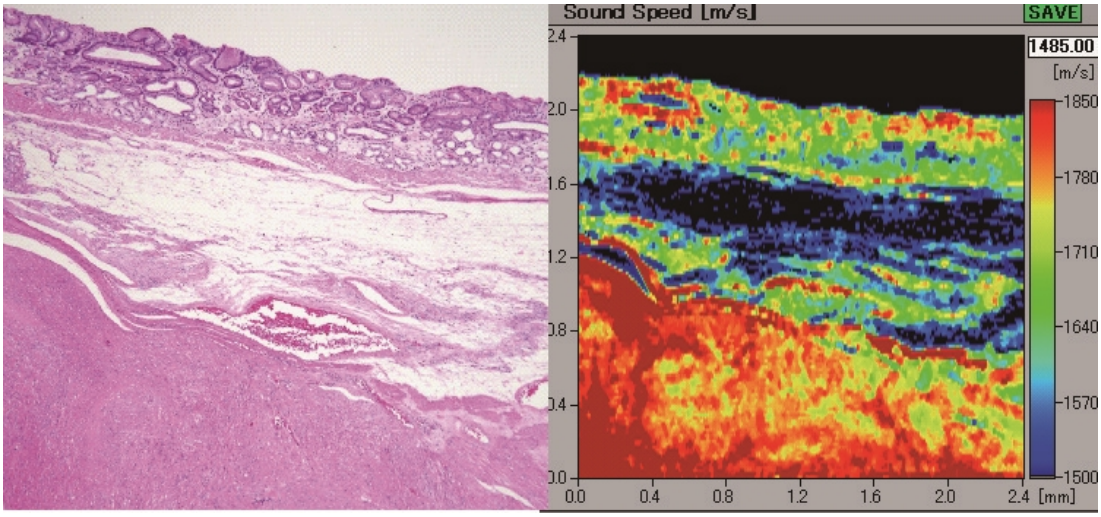

Fig. 7C. A leiomyoma with dense muscle bundles

The highest speed-of-sound values (right) were observed from the mucosa to the muscularis externa.

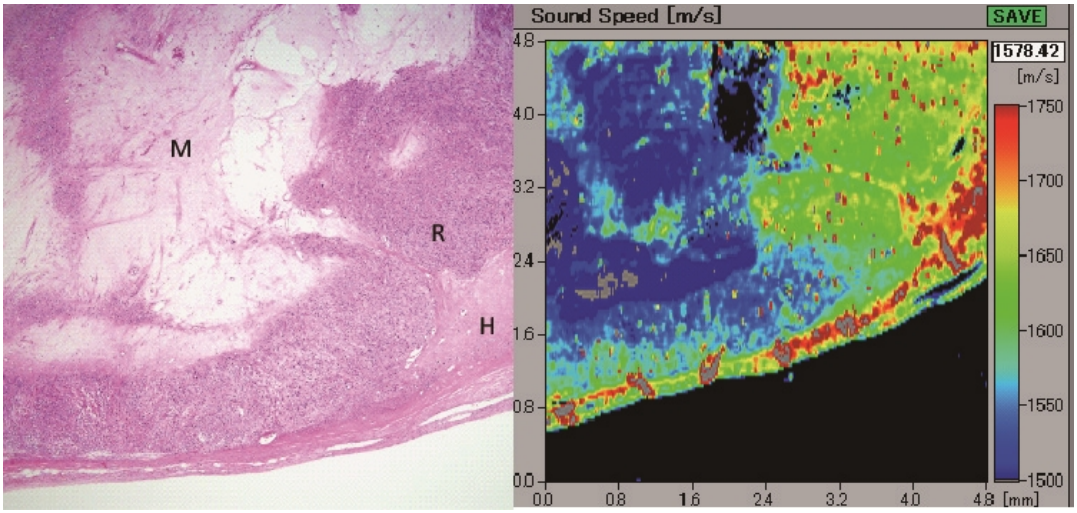

Fig. 8A. A leiomyosarcoma with myxoid areas

The hyalinized area (H), tumor cell-rich area (R), and myxoid transition area (M) display the highest, middle, and lowest speed-of-sound values, respectively. The hot spots in the cell-rich area correspond to blood vessels.

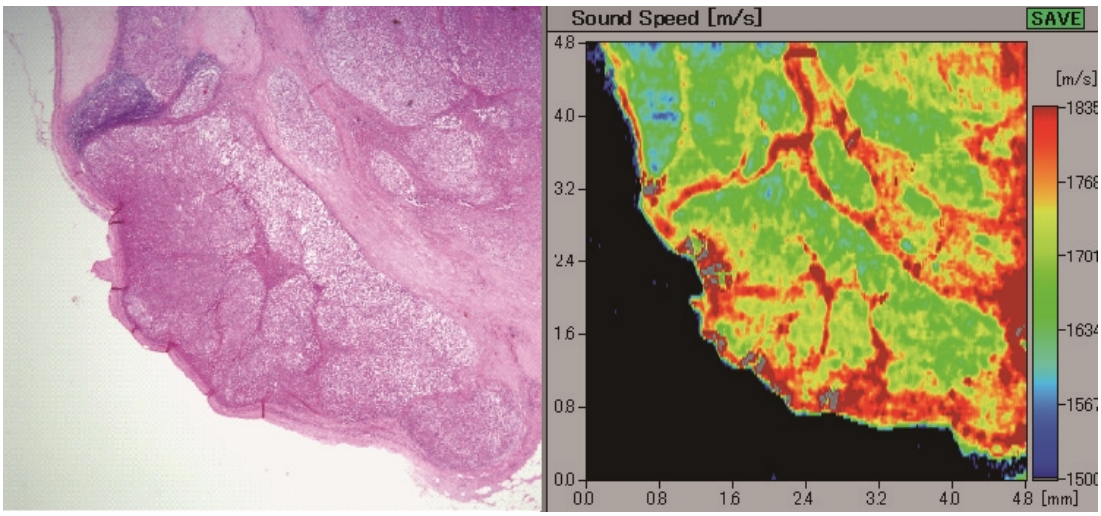

Fig. 8B. A gastric leiomyosarcoma comprising multinodular structures with irregular outer contours

The nodules are made up of tumor cells that are separated by a fibrous band and exhibit lower speed-of-sound than the fibrous band.

3.6 GIST

GISTs of the stomach formed large submucosal nodules, and their SOS values were almost identical to those measured in the mucosa (Figs. 9A and 9B, Table 1). Focal areas with myxoid change exhibited lower SOS values than cell-rich areas.

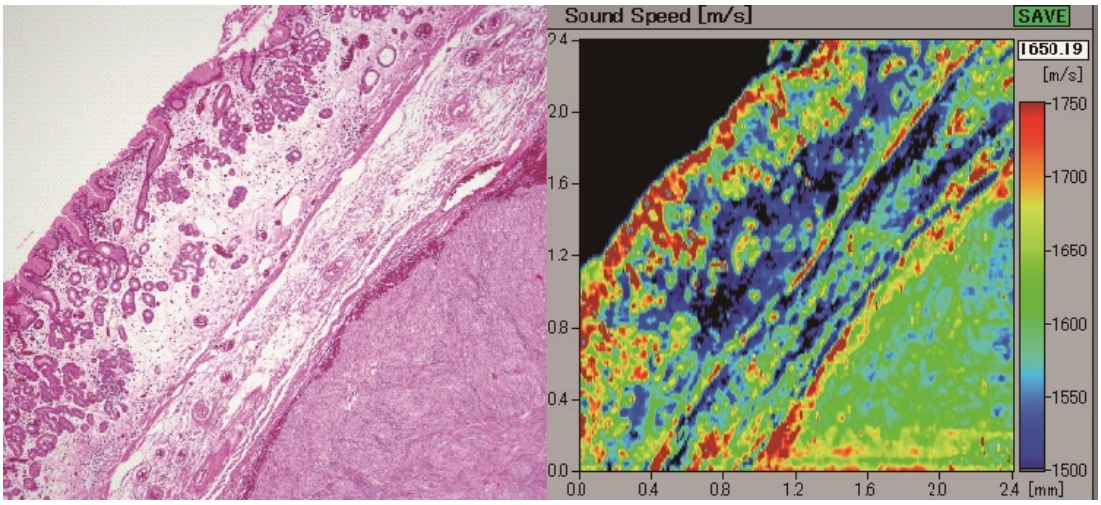

Fig. 9A. A gastrointestinal stromal tumor in the submucosa

The tumor margin has numerous blood vessels and shows higher speed-of-sound (SOS), whereas the tumor center displays almost the same SOS as that of the foveolar epithelium. The mucosal surface shows greater SOS, which corresponds to rich mucousal content.

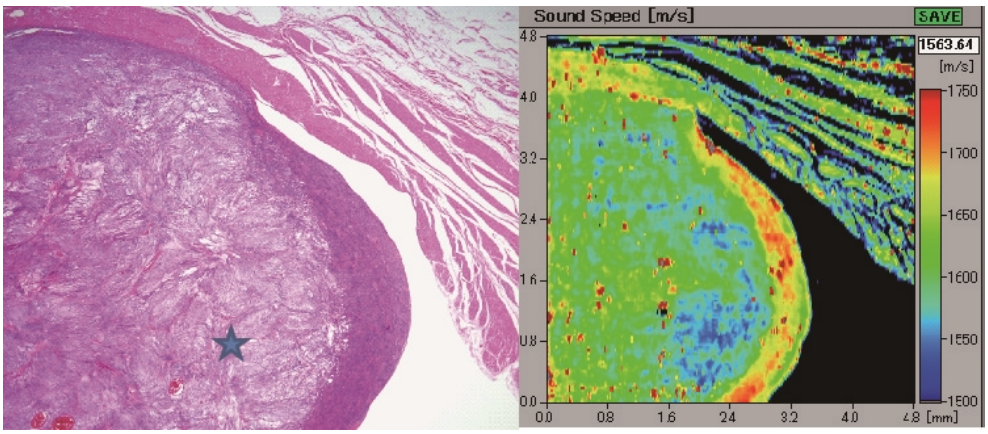

Fig. 9B. A gastrointestinal stromal tumor (GIST) protruding from the muscularis externa into the serosa

The GIST shows variable speed-of-sound (SOS) among different areas. The cell-rich serosal surface displays higher SOS and the cell-deficient central area with myxoid change (asterisk) exhibits reduced SOS. The spotty areas with increased SOS correspond to blood vessels.

3.7 Schwannomas

Schwannomas included both cell-rich and cell-deficient areas, which exhibited large and small SOS values, respectively (Fig. 10).

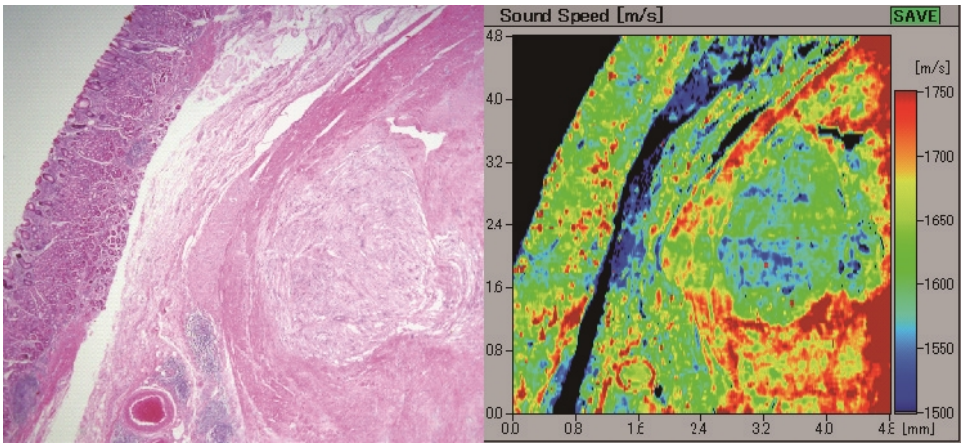

Fig. 10. A gastric schwannoma in the submucosa

The schwannoma mixed with cell-rich and cell-deficient areas demonstrate higher and lower speed-of-sound, respectively.

4. DISCUSSION

The biomedical application of SAM was first described by Lemons and Ouate [7]. SAM is a confocal imaging device in which thin specimens are scanned point-by-point using very strongly focused beams [4]. The attenuation of US in tissues is much greater than that in water and increases with elevation in the frequency.

The data on the SOS values in biological tissues in various organs can be found in reviews [8,9]. Studies of the acoustic properties of tissues at low frequency suggest that SOS values in soft tissues differ only slightly from those in water and are virtually independent of frequency. Significant differences between SOS in water and objects were only observed for solid biological tissues, such as bones and tissues that contain large concentrations of fibrillar proteins[9]. Because the stomach has muscle layers and exhibits reactive fibrosis, data from high-frequency SAM may provide useful information to complement low-frequency EUS imaging.

The abovementioned SAM results show both normal and abnormal gastric images. Normal layer structure was destroyed by various causes, including neoplastic and inflammatory lesions. Each layer or lesion is characterized by their own SOS, which is useful for discriminating lesions. On EUS imaging, five distinct layers are seen [2,3], which correspond to the following: layer 1, interface echo between the superficial mucosa and the acoustic coupling medium; layer 2, deep mucosa; layer 3, SM plus the acoustic interface between SM and ME; layer 4, ME without the acoustic interface between SM and ME; and layer 5, serosa and subserosal fat. In SAM, layer 1 corresponded to surface mucous contents; layer 2 was equivalent to MM; and layers 3 and 4 almost corresponded to SM and ME, respectively, although their interface was sometimes obscured owing to the presence of loose muscle fibers.

In a normal stomach, muscle layers such as MM and ME were harder on palpation than mucosa or SM, which were well discriminated by SAM imaging. Higher cellularity and richer fiber content owing to fibrosis and muscle bundles also exhibited greater SOS values[6]. Overall, the SOS values for each layer corresponded well to tissue elasticity.

All tissues have their own speed-of-sound (SOS) by which ultrasound travels through them. The SOS is usually proportional to the tissue elasticity. Even after formalin fixation, the specimens usually keep their elasticity in the same order as their original unfixed ones (Supplemental Fig. 1). Table 1 and Fig. 3 showed particular SOS of each lesion or component of stomach, so that imaging from SOS reflected each tissue character of objective elasticity compared with palpation hardness.

Most tumors displayed similar SOS values to their original tissues because cellular components are similar between adenocarcinoma/carcinoid and normal tubules. So carcinomas or carcinoid tumors arising from mucosa demonstrated the same SOS values as mucosal glands or tubules.

Secondary histological modifications such as necrosis, cyst formation, and fibrosis increase according to tumor development from minimal in early carcinoma to severe in advanced one.

In early carcinomas/carcinoids, no desmoplastic reactions were found in the mucosa, while at submucosal invasive sites, stromal reactions appeared and the reactivity varied among tumors. Usually more poorly differentiated cacinomas show more desmoplastic reactions to form scirrhous stroma. SAM has succeeded in imaging the desmoplastic reactions as seen in Figs. 4D and 4E.

Compared with benign leiomyomas that are conspicuously hard, leiomyosarcomas are usually softer upon palpation. The SAM data proposed significantly less SOS of leiomyosarcomas than that of leiomyomas, which confirms is in accordance with the aforementioned findings.

We used FFPE sections instead of fresh-frozen tissue. In the literature, low-frequency studies (1–7 MHz) of acoustic parameters, including SOS, have demonstrated that fixation in 4% formalin solution changed these parameters only slightly [10]. FFPE kidney tissue showed no significant differences from fresh-frozen kidney tissue [11]. Moreover, we assessed the effect of fixation effect on SAM observations before performing this study. We prepared fresh-frozen sections and soaked them in 10% formalin to observe changes in SAM findings according to the fixation duration. Because mucosal imaging was unstable before 1-h fixation (Supplemental Fig. 1), we used paraffin sections that had been fixed for more than 1 h in this study. Other merits of using FFPE included the availability of archive blocks and easy preparation of 10-μm flat sections compared with fresh-frozen sections.

Malignant tumors are, in general, harder than surrounding normal tissues. Manual palpation has been used to assist in diagnosis, but it is subjective and restricted to large and more superficial structures. In the upper GI tract, EUS has recently been used to diagnose subepithelial lesions, estimate the invasive depth of early GI cancers, and evaluate of esophageal varices [12]. For definite diagnosis of subepithelial lesions, particularly deep SM and ME layers, histological access, such as that achieved with EUS-guided fine needle aspiration, is usually needed [3]. SAM results indicated that SM non-epithelial tumors demonstrated similar SOS values. Irregular margins and geographic myxoid changes may be suggestive of malignancy, and biopsy specimens should be obtained from these sites.

An ultrasonic imaging system typically needs to be able to resolve structures of ~1 mm size at depths of up to ~150 mm in humans. US waves travel ~1500 m/s through water. The wavelength, which is one of the factors that determines spatial resolution, is optimal for abdominal scanning, for example, 0.5 mm at 3 MHz[4]. Objects smaller than the wavelength do not reflect US. The penetration length through tissues decreases proportional to the wavelength. For histological imaging, we employed a 120-MHz transducer that had about 13-μm spatial resolution, which barely allows it to detect single cells.

We previously reported SAM imaging of lungs[5] and lymph nodes[6]. In the latter, statistically significant differences in SOS values were observed among scirrhous carcinomas, lymphomas, and medullary carcinomas. The SOS values of these tumors correlated with the elasticity on manual palpation. These results were also applicable to gastric lesions. In the lung, the degree of pulmonary fibrosis was reflected with SAM and was statistically comparable between lesions. In gastric lesions, tumor invasion-induced stromal fibrosis was detected by SAM, and the SOS data revealed a statistical difference between non-invasive and invasive carcinomas.

5. CONCLUSION

In conclusion, based on our experiences and the present observation, SAM offers the following benefits over LM: (1) images are acquired in only a few minutes without the need for special stains; (2) repeated observations of the same section are possible (3) digital SOS imaging achieves high resolution, approaching that achieved with LM; (4) SAM analysis could be helpful to understand ultrasonic endoscopic images; and (5) digitized SOS data can be used to statistically compare different stomach lesions.

ACKNOWLEDGMENT

We thank Dr. K. Kobayashi (Honda Electronics Co., Ltd., Toyohashi, Japan) for his technical

support and advice regarding scanning acoustic microscopy and S. Okamoto, T. Kato, Y. Kawabata, and N. Suzuki for preparing the tissue sections. The authors would like to thank Enago (www.enago.jp) for the English language review.

This work was supported by Japan Society for the Promotion of Science KAKENHI Grant Number Scientific Research (c) 24590445.

COMPETING INTERESTS

The authors declare that they have no competing financial interests.

REFERENCES

1. Wells PNT. Velocity, absorption and attenuation in biological materials. In *Biomedical ultrasonics*. Academic Press: London. 1977;110-137.
2. Hwang JH, Rulyak SD, Kimmey MB. American Gastroenterological Association Institute technical review on the management of gastric subepithelial masses. Gastroenterology. 2006;130:2217-2228.
3. Sakamoto H, Kitano M, Kudo M. Diagnosis of subepithelial tumors in the upper gastrointestinal tract by endoscopic ultrasonography. World J Radiol. 2010;2:289-297.
4. Wells PN. Advances in ultrasound: from microscanning to telerobotics. Br J Radiol 2000;73:1138-1147.
5. Miura K, Yamamoto S. Pulmonary imaging with a scanning acoustic microscope discriminates speed-of-sound and shows structural characteristics of disease. Lab Invest. 2012;92:1760-1765.
6. Miura K, Nasu H, Yamamoto S. Scanning acoustic microscopy for characterization of neoplastic and inflammatory lesions of lymph nodes. Sci Rep 2013;3:1255; DOI 10.1038/srep01255.
7. Lemons RA, Quate CF. Acoustic microscopy: biomedical applications. Science 1975;188:905-911.
8. Chivers RC, Parry RJ. Ultrasonic velocity and attenuation in mammalian tissues. J Acoust Soc Am. 1978;63:940-953.
9. Maev R. Acoustic properties of biological tissues and their effect on the image contrast. In Acoustic microscopy, Fundamentals and application. Wiley-VCH: Weinheim, Germany. 2008;212-213.
10. Bamber JC, Hill CR, King JA, Dunn F. Ultrasonic propagation through fixed and unfixed tissues. Ultrasound Med Biol. 1979;5:159-165.
11. Sasaki H, Saijo Y, Tanaka M, Okawai H, Terasawa Y, Yambe T et al. Influence of tissue preparation on the high-frequency acoustic properties of normal kidney tissue. Ultrasound in Med and Biol. 1996;22:1261-1265.
12. Kim EY. Endoscopic ultrasound, where are we now in 2012? Clin Endosc 2012;45:321-323.

Peer-review history:
The peer review history for this paper can be accessed here:
http://www.sciencedomain.org/review-history.php?iid=268&id=5&aid=2093